Korean J. Chem. Eng., 35(7), 1570-1576 (2018)
DOI: 10.1007/s11814-018-0047-3

pISSN: 0256-1115
eISSN: 1975-7220

Improved dielectric properties and energy density of PVDF composites using PVP engineered $BaTiO_3$ nanoparticles

Yu Dai and Xiaojun Zhu†

School of Energy Science and Engineering, Central South University, Changsha, Hunan 410083, China
(*Received 16 October 2017 • accepted 15 March 2018*)

Abstract−This work systematically investigates the effect of modifier polyvinylpyrrolidone (PVP) on the microstructure, dielectric and energy storage properties of $BaTiO_3$/PVDF composites. The results demonstrate that the $BaTiO_3$ nanoparticles modified by PVP are uniformly dispersed in the composites, and the defects including cracks and voids are obviously decreased in contrast to the composites with unmodified $BaTiO_3$ nanoparticles. Due to the enhanced interfacial polarization, the composites with $BaTiO_3$@PVP show improved dielectric properties compared with the composites with unmodified $BaTiO_3$ nanoparticles. For instance, at 1 kHz, the dielectric constant and dielectric loss of the composite with 50 vol% of $BaTiO_3$@PVP nanoparticles are 80.4 and 0.085, while of which the $BaTiO_3$/PVDF are 35 and 0.265, respectively. The discharge energy density of the composites is largely improved with PVP engineered $BaTiO_3$ nanoparticles. The composite with 30 vol% $BaTiO_3$@PVP achieves a discharged energy density of 4.06 J/cc at 240 kV/mm, which is 116% larger than that of pure PVDF (1.88 J/cc). This research provides an effect modifier to prepare high performance dielectric materials.

Keywords: Dielectric Composite, Energy Density, PVP, PVDF, $BaTiO_3$

INTRODUCTION

High performance dielectric materials for high power density capacitors have been a focus for theuir potential applications in advanced electronic devices and electric power systems, such as embedded capacitors, multilayer capacitors, and gate insulators in organic field effect transistors [1-8]. Compared with the lithium battery and other renewable energy systems, dielectric composites possess the advantage in power density, while the relatively low energy density is still the bottleneck problem that limits its application [9-12]. The main parameters determining the energy density of dielectric composites are dielectric constant and breakdown strength [13-16].

Common ferroelectric ceramics, such as $BaTiO_3$ [17,18], Pb(Zr, Ti)O_3 (PZT) [19], and $Pb(Mg_{1/3}Nb_{2/3})O_3$-$PbTiO_3$ (PMN-PT) [20], usually have high dielectric constant (~>1,000) and low dielectric loss. Therefore, they are considered as an ideal dielectric material. However, due to their low breakdown strength, brittle, and poor processing performance, ceramics are often subjected to great restrictions. In contrast, polymer has excellent flexibility, high breakdown strength and low dielectric loss, but its dielectric constant is very low, generally less than 10 [21-25]. It is obvious that the single component ceramic or organic polymer is not an ideal dielectric material [25,26]. Therefore, ceramic/polymer composite is considered to be one of the most promising high-performance dielectric materials, which can combine high dielectric constant from ceramics with high breakdown strength from polymers [27-31]. However, due to the high surface energy of the ceramic powders and the poor compatibility between ceramic powders and polymer matrix, the ceramic powders easily aggregate in the composite and weakly bond with the matrix [32-34]. Unavoidable defects caused by agglomeration of ceramic particles in the composites and weak interfacial adhesion between inorganic ceramics and organic matrix would reduce the dielectric constant and increase the dielectric loss of the composites.

Recently, much attention has been focused on exploring the effects of modifiers on improving the dispersion and compatibility of ceramic fillers in the polymer matrix [35-38]. Preparation of core-shell structured ceramic fillers using living polymerization method, such as in situ atom-transfer radical polymerization (ATRP), was considered to be a potential method to improve the dispersion and compatibility problems [33,39,40]. A core-shell structured of $BaTiO_3$ hybrid nanostructures ($BaTiO_3$-HBP) using grafting hyperbranched aromatic polyamide to the surface of $BaTiO_3$ nanoparticles was reported; the dielectric properties of the composites were modulated due to the controllable core-shell structures [41]. However, this method is hard to control due to the harsh conditions and complex process. Therefore, finding a simple and effective modifier to modify the surface of ceramic fillers in large-scale application is imminent. An environmentally friendly and low-cost modifier hydantoin epoxy resin was proposed for the first time to engineer the surface of $BaTiO_3$ nanoparticles. The results showed that the modified $BaTiO_3$ nanoparticles were homogeneously dispersed in the polymer matrix, and energy storage density of the composite was obviously improved [42]. Their works give a good beginning for large-scale practical application by a simple method, while which is far from enough.

In this work, we employed a kind of common industrial raw material polyvinyl pyrrolidone (PVP) as the modifier of $BaTiO_3$ nano-

†To whom correspondence should be addressed.
E-mail: xjzhu@csu.edu.cn

particles using a simple one-step method, and provided a demonstration of its ability to enhance the dispersibility and compatibility of $BaTiO_3$ nanoparticles in polyvinylidene fluoride (PVDF) polymer matrix. Due to the improved dispersion and compatibility of $BaTiO_3$ nanoparticles, the composite achieved enhanced performance. The dielectric constant of and dielectric loss of the composite with 50 vol% of $BaTiO_3$@PVP are 80.4 and 0.085, respectively, at 1 kHz. The discharge energy density of the composites is largely improved to 4.06 J/cc, which is more than two times the pure PVDF (1.88 J/cc) at 240 kV/mm. This work provides an effective modifier for a wide range of ceramic fillers to prepare high performance polymer based capacitors.

EXPERIMENTAL SECTION

1. Materials

Polyvinyl pyrrolidone (PVP) (99.5%) and H_2O_2 (35 wt%) were purchased from Guoyao, China. $BaTiO_3$ nanoparticles with the average size of approximate 100 nm and the purity of 99.9% were purchased from Aladdin Co., Shanghai, China. Poly(vinylidene fluoride) (PVDF) polymer was provided by PolyK Technologies, LLC. All chemicals were used 'as received', unless indicated.

2. Functionalization of the $BaTiO_3$ Nanoparticles

10 grams of $BaTiO_3$ nanoparticles was added into 80 mL of H_2O_2 aqueous solution with a round-bottomed flask. The mixture is sonicated for 20 min and refluxed at 106 °C for 6 h. The nanoparticles were recovered by centrifugation at 6,000 rpm for 1 min. The obtained $BaTiO_3$ nanoparticles were washed by deionized water and dried under vacuum at 70 °C for 24 h. Subsequently, 1 gram of PVP was dissolved in ethanol and mixed with 10 g of H_2O_2 treated $BaTiO_3$ nanoparticles, and stirred for 10 min. The solution was stirred for 24 h at room temperature to ensure that the $BaTiO_3$ nanoparticles were completely coated by PVP. After that, the suspension was centrifuged for 3 min at 6,000 rpm and dried at 70 °C for 24 h.

3. Preparation of $BaTiO_3$@PVP/PVDF Composites

PVDF can be effectively dissolved in the mixed solvent of acetone and DMF. Acetone is a kind of solvent with low boiling point (approximately 56 °C), which is much lower than that of DMF. Therefore, the acetone will be rapidly volatilized during the process of drying, which can prevent the $BaTiO_3$ nanoparticles from settling as far as possible. Therefore, the mixed solvent of acetone and DMF ($V_{acetone}$: V_{DMF}=7 : 3) was selected as the solvent PVDF. The detailed experimental section is shown in Fig. 1. First, 4 grams of PVDF was added into 46 g as-prepared component solvent ($V_{acetone}$: V_{DMF}=7 : 3) and the solution was stirred at 40 °C until it is transparent. Then, the $BaTiO_3$@PVP particles were added into the PVDF solution to prepare the suspensions with the loadings of 10, 20, 30, 40 and 50 vol%, respectively. Secondly, the suspensions were all stirred for another 24 h to obtain homogeneous suspension. Subsequently, the composite films were prepared using tape-casting method on a glass substrate and dried at 80 °C. The films were further hot-pressed at 200 °C and 15 MPa. The Au electrodes were sputtered on the surface of the composites using the metal mask with a diameter of 2 mm, and the thickness of the samples was approximately 20 μm. In contrast, composites with unmodified $BaTiO_3$ nanoparticles were prepared. The detailed process is as follows: the purchased $BaTiO_3$ nanoparticles without any treatment were added into the PVDF solution to prepare the suspensions with the loadings of 10, 20, 30, 40 and 50 vol%, respectively. Secondly, the suspensions were all stirred for another 24 h to obtain a homogeneous suspension. Subsequently, the composite films awere prepared using tape-casting method on a glass substrate and dried at 80 °C. The films were further hot-pressed at 200 °C and 15 MPa.

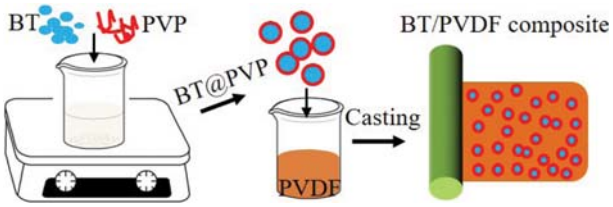

Fig. 1. Schematic illustration of process for $BaTiO_3$@PVP/PVDF composites.

4. Characterization

The microstructure of the composites was observed by a scanning electron microscope (SEM, Nova NanoSEM230, USA). Transmission electron microscopy (TEM, Titan G260-300) was taken to observe the morphology of $BaTiO_3$ and PVP modified $BaTiO_3$ nanoparticles, using an accelerating voltage of 300 kV. Fourier-transform infrared (FT-IR, Nicolet 6700) spectroscopy was performed over the range of 4,000-450 cm^{-1} to determine the functionalization of $BaTiO_3$ nanoparticles. Thermogravimetric analysis (TGA, NET-ZSCH STA 449) was conducted at a heating rate of 10 °C/min in a nitrogen flow (20 mL/min). Frequency-dependent permittivity and dielectric loss were measured using an Agilent 4294A LCR meter with the frequency ranging from 1 kHz to 10 MHz. Electric displacement-electric field loops and leakage current were measured by a Precision Premier II ferroelectric polarization tester (Radiant, Inc.) at room temperature and 10 Hz.

RESULTS AND DISCUSSION

Fourier-transform infrared spectrum (FT-IR) was used to con-

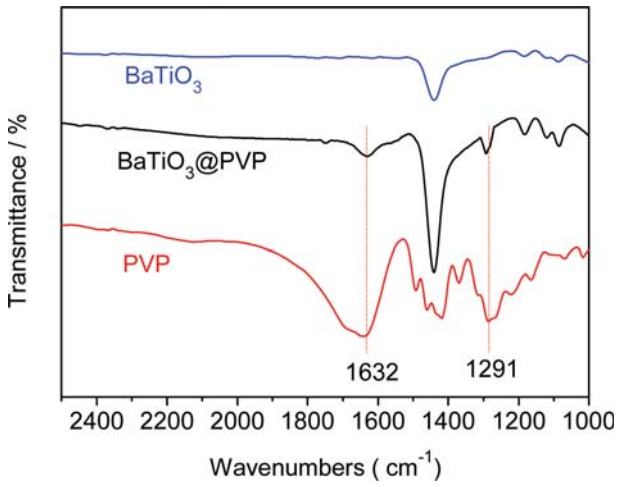

Fig. 2. FT-IR spectra of $BaTiO_3$, $BaTiO_3$@PVP and PVP.

firm that the PVP was successfully coated on the surface of $BaTiO_3$ nanoparticles (results are shown in Fig. 2). There was no characteristic peak detected in the range from 1,800-1,600 and 1,400-1,200 cm^{-1} in curve of $BaTiO_3$. In contrast, after the $BaTiO_3$ nanoparticles were modified by PVP, two obvious peaks at 1,632 and 1,291 cm^{-1} were detected, respectively, which originated from -C=O vibrational transition, and -C-N- stretching vibrations from the PVP, and two peaks were also detected at the same wavenumbers in the curve of the PVP sample. These results indicate that the PVP was successfully coated on the surface of $BaTiO_3$ nanoparticles.

Transmission electron microscope (TEM) images were used to observe the morphology of $BaTiO_3$ nanoparticles and PVP modified $BaTiO_3$ nanoparticles. Fig. 3(a) shows the TEM bright field images of the $BaTiO_3$@PVP nanoparticles. As can be seen, the average diameter of the $BaTiO_3$ nanoparticles is ~100 nm, and an obvious resin layer can be found on the surface of every $BaTiO_3$ nanoparticles, which can be distinguished by the different colors. The coated layer can be further confirmed by the high resolution transmission electron microscopy (HR-TEM) image due to the different lattice fringes. The PVP layer is amorphous, which can be easily distinguished with a thickness of approximately 5 nm. In contrast, the TEM images of $BaTiO_3$ nanoparticles without modification are shown in Fig. 2(c) and 2(d), which can further help to distinguish the PVP layer. These results further prove that PVP was successfully coated on the surface of $BaTiO_3$ nanoparticles.

The sectional scanning electron microscope (SEM) images of the composites with $BaTiO_3$@PVP, and unmodified $BaTiO_3$ are shown in Fig. 4(a) and 4(b), respectively. As can be seen, the $BaTiO_3$ nanoparticles modified by PVP are embedded in the polymer matrix and show excellent dispersibility in the composite. Obviously de-

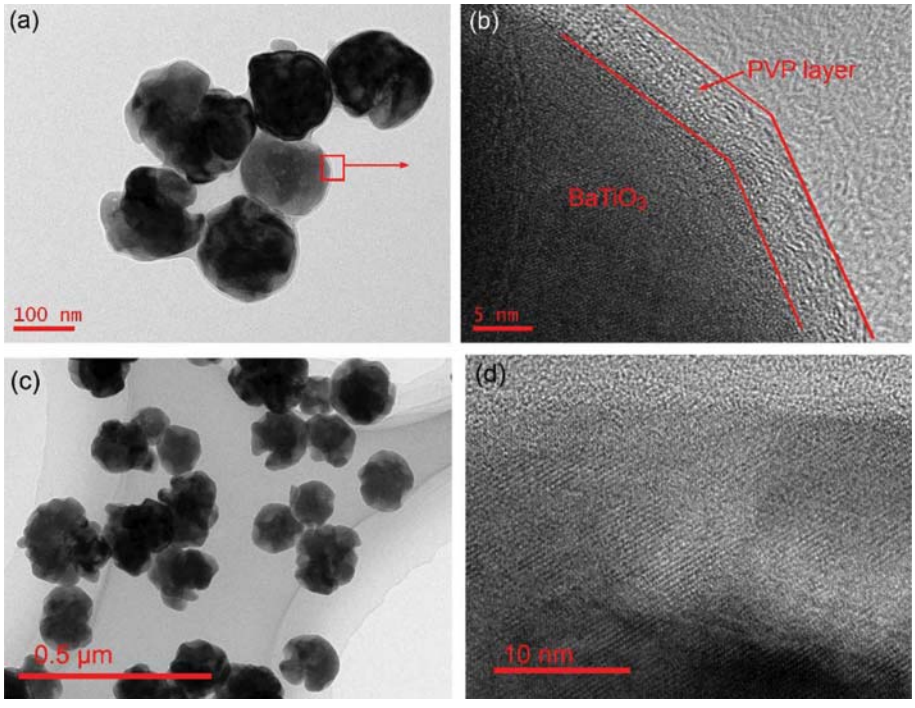

Fig. 3. (a) TEM images and (b) high-resolution TEM images of $BaTiO_3$@PVP nanoparticles, (c) TEM images and (d) high-resolution TEM images of $BaTiO_3$ nanoparticles.

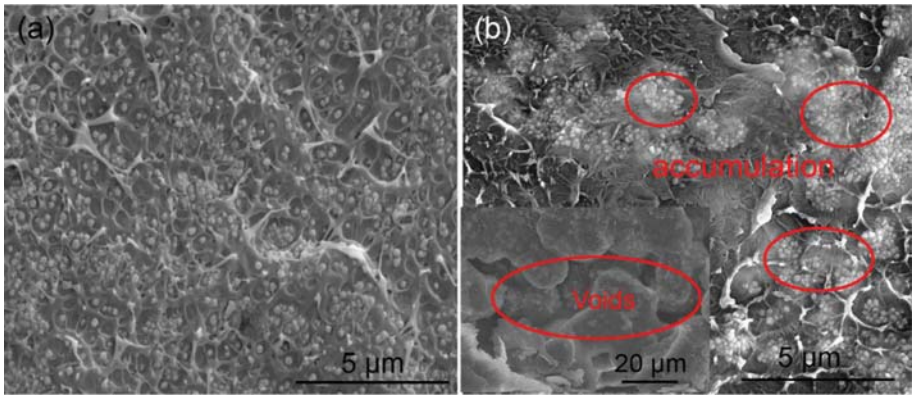

Fig. 4. Sectional SEM images of the composites with (a) $BaTiO_3$@PVP, and (b) unmodified $BaTiO_3$ nanoparticles.

creased defects including agglomeration and voids are found in the composites with $BaTiO_3$@PVP, which is beneficial from the PVP layer. Because the oxygen atom from the PVP can form hydrogen bond with the hydrogen atom from the matrix; thus the PVP can adhere to the matrix tightly [42,43]. In contrast, due to the difference of surface energy between $BaTiO_3$ nanoparticles and PVDF matrix, the unmodified $BaTiO_3$ nanoparticles are seriously accumulated in the composites, and voids and cracks are clearly found in the composites, as shown in Fig. 4(b) and the insert image. The results indicate that PVP is an effective modifier for ceramic particles.

It has been proved that in 0-3 composites (polymer composite with spherical ceramic nanoparticles), the relative permittivity will increase with increasing $BaTiO_3$ nanoparticles followed by a maximum in the permittivity at around 50-60 vol%, after which the permittivity will decrease rapidly with further increase of the nanoparticles loadings [44]. In addition, the composites with high ceramic loadings will lead to high mass density, low flexibility and poor mechanical performance [45]. Therefore, the maximum volume ratio of $BaTiO_3$ nanoparticles is 50%. Fig. 5 displays the results of the dielectric properties of $BaTiO_3$@PVP/PVDF and $BaTiO_3$/PVDF composites with different $BaTiO_3$ loadings.

Fig. 5(a) and 5(b) are the frequency-dependent dielectric constant and the dielectric loss over the range of 1 kHz to 10 MHz of the composites with $BaTiO_3$@PVP, respectively. The dielectric constant of the composites increases with the loadings of the $BaTiO_3$@PVP. For example, the dielectric constant of the composite increases to 80.4 at 1 kHz when the loading of $BaTiO_3$@PVP is 50 vol%, which is more than eight-times the PVDF (9.5 at 1 kHz), and the dielectric loss is still as low as 0.085 due to the $BaTiO_3$@PVP nanoparticles being embedded in the polymer matrix with excellent dispersibility in the composites. In addition, the dielectric constant of composites decreases gradually with the increase of frequency, which is especially obvious when the $BaTiO_3$@PVP loading is up to 50 vol%. For example, the dielectric constant of the composite with 50 vol% $BaTiO_3$@PVP is 80.4 at 1 kHz, and the dielectric constant is reduced to 53.0 at 1 MHz. This is the result of the existence of electrical conductivity in the materials [46]. The interfacial polarization is mainly in the low frequency region., the interfacial polarization decreases with the frequency increases. In contrast, the dielectric constant and dielectric loss of the composite with unmodified $BaTiO_3$ nanoparticles are shown in Fig. 5(c) and 5(d), respectively. The obvious features are that the dielectric constant is lower than that of composites with $BaTiO_3$@PVP at the same condition. The dielectric constant of the composites is mainly attributed to the Maxwell-Wagner-Sillars (MWS) interfacial effects [47]; the unmodified $BaTiO_3$ nanoparticles are seriously accumulated in the composites, which form less interfacial area and interfacial polarization. The high dielectric loss is due to accumulated unmodified $BaTiO_3$ nanoparticles in the composites leading to a large number of defects such as holes and cracks in the composites.

The breakdown strength of the composites with various loadings of $BaTiO_3$@PVP nanoparticles is shown in Fig. 6, which was analyzed with a two-parameter Weibull distribution function via the equation: $P(E)=1-\exp[-(E/E_0)^{\beta}]$, where P(E) is the cumulative

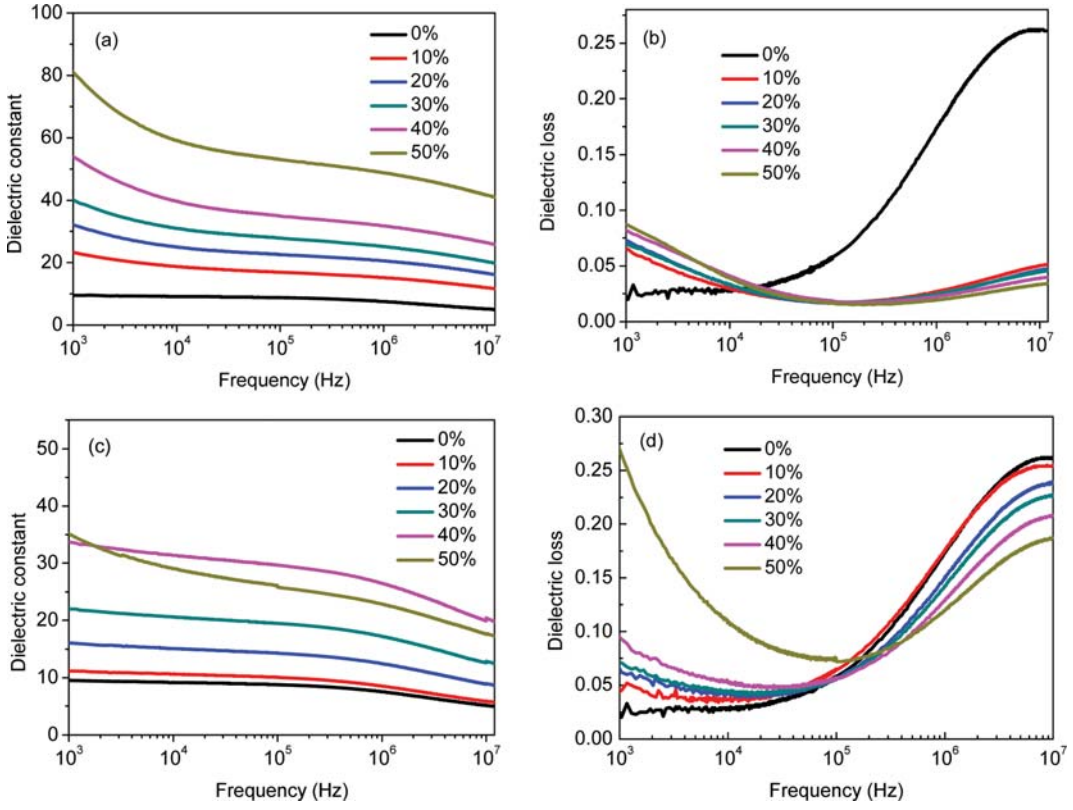

Fig. 5. Frequency dependence of (a) dielectric constant and (b) dielectric loss of the $BaTiO_3$@PVP/PVDF composites, (c) dielectric constant and (d) dielectric loss of the $BaTiO_3$/PVDF composites at room temperature.

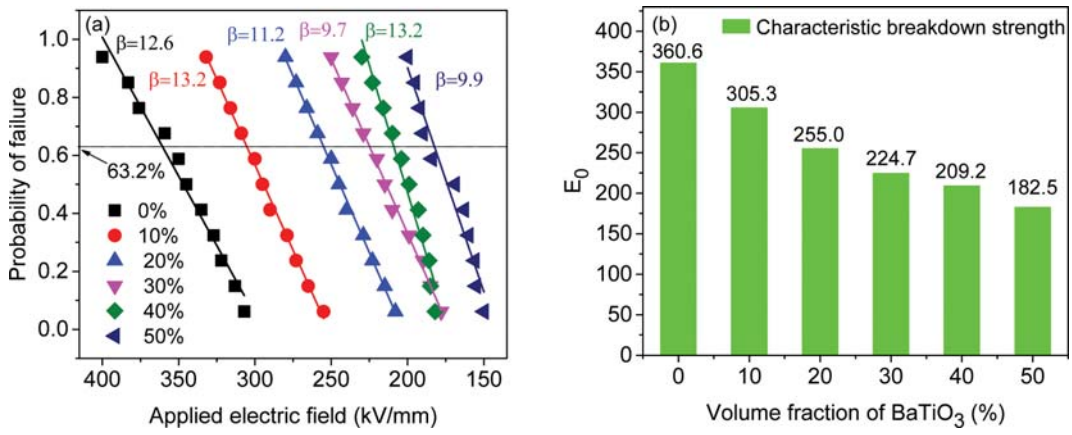

Fig. 6. (a) Weibull distribution of the breakdown strength of composites with various $BaTiO_3$@PVP nanoparticles, (b) the characteristic breakdown strength from Weibull distribution of the samples.

probability of electric failure, E is experimental breakdown strength, and E_0 is the characteristic breakdown strength, which is also the value of applied electric field on the samples when their cumulative probability of electric failure reach 63.2%. β is the shape parameter. X axis parameters are derived from the breakdown strength of all the measured samples with an ascending order and Y axis parameters are derived from the cumulative probability of electric failure of the samples calculated from the equation $P_i=(i-0.44)/(n+0.25)$, where i is the order number of the measured samples and n is the number of the measured samples [48,49]. Eleven samples were measured for each composite with different $BaTiO_3$ loadings, as shown in Fig. 6(a). The pure PVDF has the highest characteristic breakdown strength value of 360.6 kV/mm, and which is monotonically decreased with the increase of $BaTiO_3$@PVP loadings, e.g., the characteristic breakdown strength is decreased to 224.7 with 30 vol% $BaTiO_3$@PVP nanoparticles. Unavoidable defects will form with the increase of $BaTiO_3$@PVP loadings, which is the main reason that lead to the decrease of breakdown strength.

Fig. 7(a) exhibits a typical P-E loop of the nonliner dielectric materials, in which the saturation polarization (Ps) and remanent polarization (Pr) are defined. In addition, much other information is shown, such as the blue color region area represents the discharged energy density (U_d) value, and the orange region area represents the energy loss, the stored energy density inludes the discharged energy density and energy loss (U_{loss}). The insert image is the stucutre of capacitor device, which includes the electrode layer and dielectric materials central layer. Fig. 7(b) shows the results of discharged energy density and energy efficiency of the composites with the $BaTiO_3$@PVP loading and applied electric field. The U_d is calculated from the polarization-electric (P-E) loops according to the equation $U_d=\int EdD$, where D is the electric displacement, E is the applied electric field [50,51]. As can be seen the composites with higher $BaTiO_3$@PVP loading achieve higher discharged energy density due to the higher dielectric constant and higher polarization at the same electric field. The composite with 30 vol% $BaTiO_3$@PVP achieved a discharge energy density of 4.06 J/cc, which is much higher than that of pure PVDF (1.88 J/cc) at 240 kV/mm. Energy efficiency (η) is also a key parameter for the dielectrics, and the eqution is defined as: $\eta=U_d/(U_d+U_{loss})$. Although the η decreased with the increase of applied electric field and $BaTiO_3$@PVP loading due to the high energy loss, the composites possess relative high energy efficiency, such as the composite with 30 vol% $BaTiO_3$@PVP achieves an energy efficiency of 55.2% at 240 kV/mm. The results showed that composites with $BaTiO_3$@PVP nanoparticles simulta-

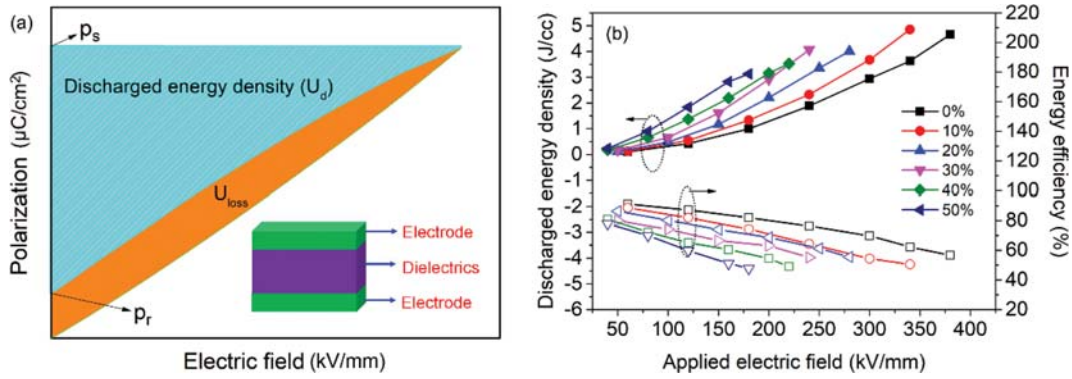

Fig. 7. (a) Typical P-E loops (the insert image is the capacitor device structure) and (b) the discharged energy density and energy efficiency of the composites with the $BaTiO_3$@PVP loading and applied electric field.

Table 1. Comparison of performance for dielectric composites with different modifiers at applied electric field

Matrix	Fillers	Modifier	Dielectric constant	Dielectric loss	U_{dis} (J/cm^3)	η (%)	Ref.
P(VDF-HFP)	$BaTiO_3$	Paraffin	60.8	0.06	2.09	9.95	37
P(VDF-HFP)	PMN-PT	Dopamine	65.1	0.037	1.02	/	20
P(VDF-HFP)	$BaTiO_3$	PHFDA	~45	0.02	~2.7	/	33
P(VDF-HFP)	$BaTiO_3$	PFBPA	~32	~0.03	3.2	/	44
P(VDF-HFP)	$BaTiO_3$@TiO_2	Dopamine	14.7	0.037	2.8	~30	13
PVDF	$BaTiO_3$	PVP	80.4	0.085	4.06	55.2	This work

neously obtained high energy density and energy efficiency. Table 1 summarizes the performance of some typical dielectric composites with the electric field, which indicates that PVP is an effective modifier for high performance dielectric composites.

CONCLUSIONS

Polyvinylpyrrolidone (PVP) is employed as the modifier of $BaTiO_3$ nanoparticles for energy storage application, of which the ability of improving the dispersibility and compatibility of $BaTiO_3$ nanoparticles in the PVDF composites and enhancing the energy density are proved. The results show that the composite with $BaTiO_3$@PVP showed improved dielectric constant compared with the composite with unmodified $BaTiO_3$ nanoparticles, and the discharge energy density of the composites was largely improved with the PVP engineered $BaTiO_3$. A high discharge energy density of 4.06 J/cc and energy efficiency of 55.2% were simultaneously obtained when the composite was incorporated with 30 vol% $BaTiO_3$@PVP at 240 kV/mm. This research proves that PVP is an effective modifier for a wide range of ceramic particles in ceramic/polymer composites.

ACKNOWLEDGEMENTS

This work was financially supported by the Educational reform project of Hunan Provincial Education Department (no. 04A06).

REFERENCES

1. F. Liu, Q. Li, J. Cui, Z. Li, G. Yang, Y. Liu, L. Dong, C. Xiong, H. Wang and Q. Wang, *Adv. Funct. Mater.*, **27**, 1606292 (2017).
2. Z. Pan, L. Yao, J. Zhai, D. Fu, B. Shen and H. Wang, *ACS Appl. Mater. Interfaces*, **9**, 4024 (2017).
3. G. Wang, X. Huang and P. Jiang, *ACS Appl. Mater. Interfaces*, **9**, 7547 (2017).
4. Y. Hao, X. Wang, K. Bi, J. Zhang, Y. Huang, L. Wu, P. Zhao, K. Xu, M. Lei and L. Li, *Nano Energy*, **31**, 49 (2017).
5. D. Zhang, W. Liu, L. Tang, K. Zhou and H. Luo, *Appl. Phys. Lett.*, **110**, 133902 (2017).
6. Z. Cai, X. Wang, B. Luo, W. Hong, L. Wu and L. Li, *Compos. Sci. Technol.*, **145**, 105 (2017).
7. S. Luo, Y. Shen, S. Yu, Y. Wan, W. Liao, R. Sun and C. Wong, *Energy Environ. Sci.*, **10**, 137 (2017).
8. Z. Y. Jiang, G. P. Zheng, X. C. Zheng and H. Wang, *Polymers*, **9**, 315 (2017).
9. H. Luo, J. Roscow, X. Zhou, S. Chen, X. Han, K. Zhou, D. Zhang and C. R. Bowen, *J. Mater. Chem. A*, **5**, 7091 (2017).
10. B. Xie, H. Zhang, Q. Zhang, J. Zang, C. Yang, Q. Wang, M. Li and S. Jiang, *J. Mater. Chem. A*, **5**, 6070 (2017).
11. H. Zhu, Z. Liu and F. Wang, *J. Mater. Sci.*, **52**, 5048 (2017).
12. W.-B. Li, D. Zhou and L.-X. Pang, *Appl. Phys. Lett.*, **110**, 132902 (2017).
13. Q. Huang, H. Luo, C. Chen, X. Zhou, K. Zhou and D. Zhang, *J. Alloy Compd.*, **696**, 1220 (2017).
14. D. Zhang, W. W. Liu, R. Guo, K. C. Zhou and H. Luo, *Adv. Sci.*, **5**, 1700512 (2018).
15. Q. Li, F. Liu, T. Yang, M. R. Gadinski, G. Zhang, L.-Q. Chen and Q. Wang, *Proc. Natl. Acad. Sci. U.S.A.*, **113**, 9995 (2016).
16. R. Su, Z. Luo, D. Zhang, Y. Liu, Z. Wang, J. Li, J. Bian, Y. Li, X. Hu and J. Gao, *J. Phys. Chem. C*, **120**, 11769 (2016).
17. H. Luo, D. Zhang, L. Wang, C. Chen, J. Zhou and K. Zhou, *RSC Adv.*, **5**, 52809 (2015).
18. D. Zhang, X. Zhou, J. Roscow, K. Zhou, L. Wang, H. Luo and C. R. Bowen, *Sci. Rep.*, **7**, 45179 (2017).
19. H. Tang, Y. Lin and H. A. Sodano, *Adv. Energy Mater.*, **2**, 469 (2012).
20. H. Luo, C. Chen, K. Zhou, X. Zhou, Z. Wu and D. Zhang, *RSC Adv.*, **5**, 68515 (2015).
21. X. Lin, P. Hu, Z. Jia and S. Gao, *J. Mater. Chem. A*, **4**, 2314 (2016).
22. H. Luo, Z. Wu, C. Chen, C. Ma, K. Zhou and D. Zhang, *Compos. Part A*, **86**, 57 (2016).
23. H. Luo, K. Zhou, C. Bowen, F. Zhang, A. Wei, Z. Wu, C. Chen and D. Zhang, *Adv. Mater. Interfaces*, **3**, 1600157 (2016).
24. Z. Pan, L. Yao, J. Zhai, B. Shen, S. Liu, H. Wang and J. Liu, *J. Mater. Chem. A*, **4**, 13259 (2016).
25. X. Zhang, Y. Shen, Z. Shen, J. Jiang, L. Chen and C.-W. Nan, *ACS Appl. Mater. Interfaces*, **8**, 27236 (2016).
26. S. Peng, Q. Zeng, X. Yang, J. Hu, X. Qiu and J. He, *Sci. Rep.*, **6**, 38978 (2016).
27. G. Zhang, D. Brannum, D. Dong, L. Tang, E. Allahyarov, S. Tang, K. Kodweis, J. K. Lee and L. Zhu, *Chem. Mater.*, **28**, 4646 (2016).
28. X. Zhang, Y. Shen, B. Xu, Q. Zhang, L. Gu, J. Jiang, J. Ma, Y. Lin and C. W. Nan, *Adv. Mater.*, **28**, 2055 (2016).
29. L. Yao, Z. Pan, S. Liu, J. Zhai and H. D. Chen, *ACS Appl. Mater. Interfaces*, **8**, 26343 (2016).
30. P. Hu, Y. Song, H. Liu, Y. Shen, Y. Lin and C.-W. Nan, *J. Mater. Chem. A*, **1**, 1688 (2013).
31. D. Zhang, C. Ma, X. Zhou, S. Chen, H. Luo, C. R. Bowen and K. Zhou, *J. Phys. Chem. C*, **121**, 20075 (2017).
32. L. Xie, X. Huang, K. Yang, S. Li and P. Jiang, *J. Mater. Chem. A*, **2**, 5244 (2014).
33. K. Yang, X. Huang, Y. Huang, L. Xie and P. Jiang, *Chem. Mater.*,

25, 2327 (2013).
34. F. Liu, Q. Li, Z. Li, Y. Liu, L. Dong, C. Xiong and Q. Wang, *Compos. Sci. Technol.*, **142**, 139 (2017).
35. Y. Li, M. Fan, K. Wu, F. Yu, S. Chai, F. Chen and Q. Fu, *Compos. Part A*, **73**, 85 (2015).
36. Y. Song, Y. Shen, P. Hu, Y. Lin, M. Li and C. W. Nan, *Appl. Phys. Lett.*, **101**, 152904 (2012).
37. D. Zhang, Z. Wu, X. F. Zhou, A. Q. Wei, C. Chen and H. Luo, *Sensor. Actuat. A*, **260**, 228 (2017).
38. Q. Chen, Y. Shen, S. Zhang and Q. M. Zhang, *Annu. Rev. Mater. Res.*, **45**, 433 (2015).
39. H. Luo, C. Ma, X. Zhou, S. Chen and D. Zhang, *Macromolecules*, **50**, 5132 (2017).
40. K. Yang, X. Huang, M. Zhu, L. Xie, T. Tanaka and P. Jiang, *ACS Appl. Mater. Interfaces*, **6**, 1812 (2014).
41. L. Xie, X. Huang, Y. Huang, K. Yang and P. Jiang, *ACS Appl. Mater. Interfaces*, **5** 1747 (2013).
42. H. Luo, D. Zhang, C. Jiang, X. Yuan, C. Chen and K. Zhou, *ACS Appl. Mater. Interfaces*, **7**, 8061 (2015).
43. K. Yu, Y. J. Niu, Y. C. Zhou, Y. Y. Bai and H. Wang, *.J. Am. Ceram. Soc.*, **96**, 2519 (2013).
44. P. Kim, N. M. Doss, J. P. Tillotson, P. J. Hotchkiss, M. J. Pan, S. R. Marder, J. Y. Li, J. P. Calame and J. W. Perry, *ACS Nano*, **3**, 2581 (2009).
45. H. X.Tang, Z. Zhou and H. A. Sodano, *ACS Appl. Mater. Interfaces*, **6**, 5450 (2014).
46. D. P. Almond and C. R. Bowen, *Phys. Rev. Lett.*, **92**, 157601 (2004).
47. L. L. Sun, B. Li, Y. Zhao, G. Mitchell and W. H. Zhong, *Nanotechnology*, **21**, 305702 (2010).
48. Z. H. Yao, Z. Song, H. Hao, Z. Y. Yu, M. H. Cao, S. J. Zhang, M. T. Lanagan and H. X. Liu, *Adv. Mater.*, **29**, 1601727 (2017).
49. Y. Thakur, T. Zhang, C. Iaco, T. Yang, J. Bernhol, L. Q. Chen, J. Runt and Q. M. Zhang, *Nanoscale*, **9**, 10992 (2017).
50. S. Liu, S. Xue, W. Zhang, J. Zhai and G. Chen, *J. Mater. Chem. A*, **2**, 18040 (2014).
51. X. Huang and P. Jiang, *Adv. Mater.*, **27**, 546 (2015).